Applied Catalysis B: Environmental 94 (2010) 27–37

Contents lists available at ScienceDirect

Applied Catalysis B: Environmental

journal homepage: www.elsevier.com/locate/apcatb

Catalytic combustion of methane on nano-structured perovskite-type oxides fabricated by ultrasonic spray combustion

Xun Wei [a,1], Paul Hug [a], Renato Figi [b], Matthias Trottmann [a], Anke Weidenkaff [a], Davide Ferri [a,*]

[a] Empa, Swiss Federal Laboratories for Materials Testing and Research, Laboratory for Solid State Chemistry and Catalysis, Ueberlandstrasse 129, CH–8600 Dübendorf, Switzerland
[b] Empa, Swiss Federal Laboratories for Materials Testing and Research, Laboratory for Analytical Chemistry, Ueberlandstrasse 129, CH–8600 Dübendorf, Switzerland

ARTICLE INFO

Article history:
Received 18 August 2009
Received in revised form 9 October 2009
Accepted 17 October 2009
Available online 29 October 2009

Keywords:
Ultrasonic spray combustion
Perovskites
Methane combustion
Hollow particles
Palladium

ABSTRACT

The synthesis of perovskite-type oxides using ultrasonic spray combustion (USC) was investigated by adjusting the composition of the precursor solution and the temperature of synthesis and calcination. $LaMnO_3$ was chosen as model perovskite to systematically analyze the effect of USC operating parameters. XRD, IR spectroscopy, TG-TPD, SEM, TEM and BET were used to characterize the samples with respect to phase composition, thermal stability, morphology and surface area. The catalytic properties were evaluated with respect to methane combustion as such materials are potential catalysts in the control of exhaust gases from mobile and stationary sources. Addition of citric acid to the precursor solution and calcination in air appeared to be the crucial parameters to produce spherical hollow particles composed of nano-sized $LaMnO_3$ crystallites (down to 30 nm) with high catalytic activity and durability. Calcination was required in order to remove uncombusted precursors and to improve both the crystallinity of the materials and their catalytic activity. $LaFeO_3$, $LaCoO_3$ and $La(M,Pd)O_3$ (M = Mn, Fe) with pure perovskite-phase were synthesized in a single step under the optimal conditions selected for $LaMnO_3$. Though the order of catalytic activity within the two series of samples (with and without Pd) agreed with reported trends, the production of each single perovskite composition by USC may require further optimization around these synthesis conditions. We demonstrate that USC is a simple, versatile and reliable method with potential application in the one-step synthesis of heterogeneous catalysts.

1. Introduction

Perovskite-type oxides of general formula ABO_3, in which A is usually an alkaline earth metal or a lanthanide ion and B a transition metal ion, are well-known materials with attractive physical and chemical properties, covering magnetic and (thermo)electric properties, catalytic properties and oxygen transport capability [1,2]. Recently, perovskites have received renewed interest as catalysts for the abatement of exhaust gases from mobile and stationary sources [3–5], and seem to be able to maintain the original premise [6,7] for the control of automotive emissions.

Activity and stability of catalysts are strongly related to material properties such as particle size distribution, morphology and crystallinity that are on their turn controlled by the method of synthesis [8,9]. The classic solid state procedure for the preparation of perovskite-type oxides, involving mechanical grinding of binary oxides, presents the disadvantages of long processing time, low surface area, large particle size and limited degree of chemical homogeneity. In recent years, considerable interest has been paid to the development of suitable chemical solution methods [10–16], which can provide products of fine and homogeneous particles with relatively high specific surface area at low calcination temperature (below 800 °C). However, most of these routes involve multi-step reactions, can be elaborated and the final products may not be phase pure, which has consequences on catalytic activity [17,18]. One-step processes are more desirable to avoid time-consuming preparation routes and to offer possibility for production scale-up. Solution combustion synthesis [19] is one such method, where an additive as urea is used to promote self-sustained combustion of the precursors solution. Solution-based aerosol processes in which the precursor solution is nebulized and decomposed (in a flame or in a furnace) [20,21] are extremely promising because of their one-step and continuous character. Among few others, Co- and Ti-containing perovskites [22–24] have been prepared by flame synthesis and their catalytic properties have been evaluated prevalently in the catalytic methane combustion with respect to activity and stability.

* Corresponding author. Tel.: +41 044 823 4609; fax: +41 044 823 4041.
E-mail address: davide.ferri@empa.ch (D. Ferri).
[1] Present address: Nanotechnology Group, ETH Zurich, Tannenstrasse 3, CH–8092 Zurich, Switzerland.

0926-3373/$ – see front matter © 2009 Elsevier B.V. All rights reserved.
doi:10.1016/j.apcatb.2009.10.017

Ultrasonic spray synthesis [20,25] has demonstrated to be a unique route for the synthesis of various materials, including supported metals [20,26], metal oxides [27–30], composite powders [26], and films [31]. Ultrasonic spray synthesis is based on the ultrasound assisted generation of micro-droplets of an aqueous precursor solution containing easily available materials (i.e., nitrates). The micro-droplets are then carried through a furnace and decomposed into particles via evaporation, combustion and sintering. Typically, the resulting particles (>0.5 μm) are spherical and exhibit hollow structure, which is of interest for applications in drug delivery, catalysis and separation technology. Hollow particles are porous and have thin walls composed of nano-sized crystallites. Ultrasonic spray synthesis allows a precise control of stoichiometry and is highly reproducible, inexpensive, scalable and uncomplicated. Moreover, it can be realized in a single step and the products have narrow size distribution and display high phase purity despite the low residence time of the droplet at high temperature. Although several synonyms are currently used for the same technique [20,32], we make use of the ultrasonic spray combustion (USC) designation because we have chosen to prepare the particles using citric acid (CA) as a fuel supporting decomposition of precursors droplets in the furnace.

Various perovskite-type mixed oxides have been already produced in the form of nano-sized powders using ultrasonic spray synthesis, and included for example $BaTiO_3$ [33–35], $CaMn_{1-x}Nb_xO_3$ [36], $La_{1-x}Ca_xTiO_3$ [32,37], $GdCo_{1-x}Cu_xO_3$ [38], $LaCrO_3$ [39] and $LaMnO_3$ [40]. To the best of our knowledge none of these perovskite-type oxides was targeted to catalytic applications. To this end, the catalytic properties of powders prepared by ultrasonic spray synthesis have been evaluated only in the case of modified TiO_2 photocatalysts [26]. The synthesis of Pt/Al_2O_3, Pt/ZrO_2 [20] and Pt/SiO_2 [41] has been also accomplished however without the mention of their possible catalytic application. Therefore, the potential of the ultrasonic spray technique for the production of heterogeneous catalysts still remains to be demonstrated. We endeavor this issue starting from the USC production of simple perovskite-type mixed oxides provided their relevance for environmental catalysis.

The most important parameters influencing the production of ceramic materials using ultrasonic spray synthesis are the flow rate of the carrier gas and therefore the residence time of the droplets in the furnace, the concentration of the precursor solution, the temperature of the furnace and the atmosphere in which decomposition occurs in the furnace. We found that the carrier gas flow, the citric acid-to-metal ions ratio and the overall solution concentration were crucial to optimize the textural properties of the thermoelectric material $La_{0.95}Ca_{0.05}Fe_{0.95}Ni_{0.05}O_3$ [42].

The aim of this paper was the systematic investigation of selected relevant parameters for the USC method, i.e. the composition and concentration of the precursor solution, the temperature of synthesis and the temperature of calcination. $LaMnO_3$ was chosen for this systematic study for the following reasons: (a) $LaMnO_3$ has been prepared using numerous synthesis methods and is therefore a suitable model material; (b) it is the base for the synthesis of numerous catalysts formulations, by substitution at both A- and B-sites including addition of precious metals; (c) it is reported among the most active perovskite-type oxides for methane combustion. The present characterization focused on the relationship between the variation of the synthesis parameters and the morphological, textural and catalytic properties of the samples. Besides, $LaFeO_3$ and $LaCoO_3$ powders were synthesized via USC after selection of the optimal conditions based on the characterization of $LaMnO_3$ samples. Finally, preliminary results have been obtained for the production of Pd-containing manganites and ferrites as these materials became increasingly attractive as potential catalysts for the removal of pollutant exhaust gases [3,5,43].

2. Experimental

2.1. Ultrasound spray combustion

The homebuilt ultrasound spray combustion (USC) equipment is composed of an atomizer, a quartz reactor, a high temperature furnace and a vacuum pump [37]. Micro-droplets of the precursor solution were generated by an ultrasonic atomizer consisting of three piezoelectric oscillators at a fixed frequency of 1.67 MHz, and then transported by a flow of synthetic air (2 l/min) through a quartz tube (l = 1300 mm; d_{ext} = 26 mm) installed in a vertical high temperature furnace (Nabertherm), where they were calcined and the one-step synthesis of the nanoparticles took place. The distance between the surface of the precursor solution and the heated zone corresponded to 55 cm, whereas the length of the heated zone and of the isothermal zone was 75 and 25 cm, respectively according to specifications of the furnace manufacturer. The relatively high flow rate of the carrier gas leads to a residence time of the micro-droplets in the furnace of about 15 s. The fine powder was collected on a membrane filter (Whatman, cellulose acetate, 0.45 μm) installed in a quartz glass pipe. A vacuum pump was used to force the powder to deposit on the filter. The production rate was ca. 250 mg/h.

Metal nitrates ($La(NO_3)_3{\cdot}6H_2O$, Fluka, >99%; $Mn(NO_3)_2{\cdot}4H_2O$, Merck, >98.5%; $Fe(NO_3)_3{\cdot}6H_2O$, Sigma–Aldrich; $Co(NO_3)_2{\cdot}6H_2O$, Merck kGaA >97%) dissolved in deionized water were used as the precursors for the perovskite-type oxides. When citric acid (CA, Riedel-de Haën, >99.5%) was used, the metal nitrates were typically added to a solution of CA in a molar ratio CA:metal ions ($M_{CA/MN}$) 2:1 and polymerized at 80 °C under constant stirring for 3 h. The obtained clear solution was then nebulized in the ultrasonic atomizer and the droplets were transferred to the furnace by means of the carrier gas. Powders were prepared at the furnace temperature of 800, 900, 1000 and 1100 °C both in the presence and in the absence of CA. $M_{CA/MN}$ was also varied from 1 to 8 in order to explore the effect of CA concentration on the morphology and the structural properties of the powders obtained by USC. The temperature at which the furnace was operated is defined as the temperature of synthesis (Ts), whereas the temperature at which calcination was carried out following synthesis is termed temperature of calcination (Tc).

$La(Mn,Pd)O_3$ and $La(Fe,Pd)O_3$ perovskite-type oxides were prepared by the addition of $Pd(NO_3)_2{\cdot}2H_2O$ (Fluka, purum) to the precursor solution containing CA ($M_{CA/MN}$ = 2) to partially substitute Mn or Fe. The final Pd loading was 2 wt.% in the case of Mn and 1 wt.% in the case of Fe. In some experiments, the precursor solution containing Pd^{2+} ions required a filtration step as a dark precipitate was formed.

A $LaMnO_3$ sample was also prepared using the amorphous citrate route [10] for the matter of comparison. The precursor solution was obtained as above by mixing the nitrate precursors with CA with $M_{CA/MN}$ = 1 (slight excess of CA). After drying in rotary evaporator at 70 °C to form a transparent gel, the precursors were dried overnight in vacuum oven at 70 °C and the resulting foam was then calcined in flowing air at 800 °C for 2 h. The specific surface area of the resulting material was 16.7 m^2/g.

2.2. Characterization

The phase purity of the synthesized nano-powders was controlled by X-ray diffraction (XRD) using a Philips X'pert Pro MPD diffractometer and Ni-filtered Cu Kα radiation. The specific surface area was determined by the BET method from the N_2 adsorption isotherms, recorded at liquid-nitrogen temperature on a BELSORP-max 30 instrument (Bel Japan). Prior to the adsorption measurements, all samples were degassed at 200 °C for 1 h. The

Table 1
Structural and catalytic properties of $LaMnO_3$ powders.

Entry	C_{MN} (mol/l)	C_{CA} (mol/l)	Ts (°C)	Tc (°C)	Morphology[a]	Surface area (m^2/g)	T_{50} (°C)[b]
1	0.1	0	800	800	Spheres (Fig. 1a)	2.4	615
2	0.1	0.1	800	800	Hollow spheres (Fig. 1b)	11.7	545
3	0.1	0.2	800	800	Hollow spheres (Fig. 1c)	21.8	515
4	0.1	0.4	800	800	Hollow spheres (Fig. 1d)	11.6	520
5	0.1	0.8	800	800	Hollow spheres (Fig. 1e)	10.9	530
6	0.2	0.4	800	–	Spheres (Fig. 2a)	38.3	500
7	0.2	0.4	800	800	Hollow spheres (Fig. 2b)	16.8	470
8	0.2	0.4	900	900	Hollow spheres (Fig. 2c)	10.8	570
9	0.2	0.4	1000	1000	Grains (Fig. 2d)	6.0	620
10	0.2	0.4	1100	1100	Grains (Fig. 2e)	2.3	ca. 700
11	0.2	0.4	1100	800	Hollow spheres (Fig. 2f)	12.5	525
12	0.1	0.2	800	–	Spheres	40.4	505
13	0.1	0.2	1100	–	Spheres	16.6	530
14	0.1	0.2	900	900	Hollow spheres	15.8	–
15	0.1	0.2	1000	1000	Grains	6.4	–
16	0.1	0.2	1100	1100	Grains	2.9	–
17	0.2	0.4	1100	–	Hollow spheres	16.1	510
18	0.2	0	800	800	Spheres	4.5	565
19	0.2	0	1100	1100	Grains	1.4	ca. 730
20	0.1	0	1100	1100	Grains	1.7	ca. 750

[a] From SEM images.
[b] Determined from catalytic measurements as indicated in Section 2.

microstructure and morphology of the powders was observed using scanning electron microscopy (SEM, JEOL JSM-6300F) and transmission electron microscopy (TEM, JEOL 200 CX). FT-IR spectra of selected samples were collected in the diffuse reflectance mode in the 4000–400 cm^{-1} spectral range using a Praying Mantis unit (Harrick) mounted within the sample compartment of a Vertex 70 spectrometer (Bruker Optics) equipped with a liquid-nitrogen cooled MCT detector. Samples were diluted with KBr and measured dry in air. Temperature programmed oxidation (TPO) experiments were carried out in a thermobalance (Netzsch, STA 409 CD) coupled to a mass spectrometer (Netzsch, Aeolus). The samples were heated to 1000 °C at a rate of 10 °C/min in flowing 20 vol.% O_2/He (50 ml/min).

The Pd content in La(Mn,Pd)O_3 and La(Fe,Pd)O_3 was determined by plasma optical emission spectrometry (ICP-OES, Varian Vista Pro Radial) after complete dissolution of the samples in aqua regia and treatment in a high-pressure asher HPA-S (240 °C, 135 bar) and addition of water (Millipore, Milli-Q Advantage A10). Measurements were repeated four times. Three placebos and two standards (ALFA Aesar) were added with 1 and 10 μg/ml metallic palladium and treated similarly. X-ray absorption near-edge spectroscopy (XANES) data of Pd-containing samples were recorded in the transmission mode around the Pd K-edge (24.35 keV) at the Swiss-Norwegian beamline (SNBL, BM01B) of the European Synchrotron Radiation Facility (ESRF), Grenoble. Samples were mixed with polyethylene and pressed in the form of pellets. The spectra were energy- and background-corrected and normalized using the WINXAS 3.1 software [44].

2.3. Catalytic activity tests

Catalytic activity measurements for methane combustion were carried out in an electrically heated quartz-tube reactor (d_i = 0.6 cm; l = 40 cm). The catalyst (100 mg) was used in the form of particles with size in the range of 150–200 μm, was diluted 1:4 with quartz (150–200 μm) and was placed in the isothermal section of the reactor between two clogs of quartz wool. Prior to reaction, the catalysts were activated in 20 vol.% O_2/He (50 ml/min) at 500 °C for 2 h. After cooling to 200 °C, the gas flow was switched to 100 ml/min of 1 vol.% CH_4/4 vol.% O_2 (balance He; GHSV ~14,150 h^{-1}). After equilibrium had been reached, the temperature was increased by 5 °C/min to 700 °C. The effluent gas was continuously analyzed with a gas chromatograph (Agilent 3000A Micro GC) equipped with PoraPlot-Q and molecular sieve 5A columns.

Table 1 summarizes the textural and catalytic properties of the various $LaMnO_3$ samples prepared in this work using USC.

3. Results and discussion

3.1. Synthesis and characterization

Fig. 1 shows the SEM images of $LaMnO_3$ powders prepared by ultrasonic spray combustion (USC) from precursor solutions with total concentration of metal ions (C_{MN}) set to 0.1 mol/l and with increasing citric acid (CA) concentration (C_{CA}), i.e., the molar ratio CA/metal ions ($M_{CA/MN}$) is 0, 1, 2, 4 and 8 from Fig. 1a, b, c, d and e, respectively.

In the absence of CA (Fig. 1a), micrometric spherical particles were produced, which had heterogeneous size in the 0.3–2.5 μm range. TEM data revealed that these particles are composed of compactly arranged perovskite primary nano-crystallites possessing a size in the range 100–200 nm (insert of Fig. 1a). Moreover, these primary particles appeared already crystalline as indicated by the presence of diffraction fringes. CA can greatly improve the particle size distribution and morphology of the products [34,40]. The addition of CA to the precursor solution induced an obvious change of morphology. First, the agglomeration of the primary nano-sized particles was prevented by adding CA. The microspheres were porous owing to the presence of large cavities and were composed of a single layer of perovskite nano-crystallites 30–50 nm in size (insert of Fig. 1c). The crystallinity of the $LaMnO_3$ nanoparticles resulted also improved compared to samples prepared without the addition of CA, which was best observed by XRD (vide infra). A substantial difference between the spherical particles obtained with and without the addition of CA is that the former ones were hollow spheres. This appears to be a general property of powders produced using ultrasonic spray synthesis [20], although contradictory results have been reported for the fabrication of La-doped $CaTiO_3$ where the use of CA caused formation of dense particles [32]. This issue appears dependent on the synthesis conditions, as large excess of CA was also found to result in the formation of dense $LaMnO_3$ particles [40], a phenomenon that we did not observe. The hollow morphology

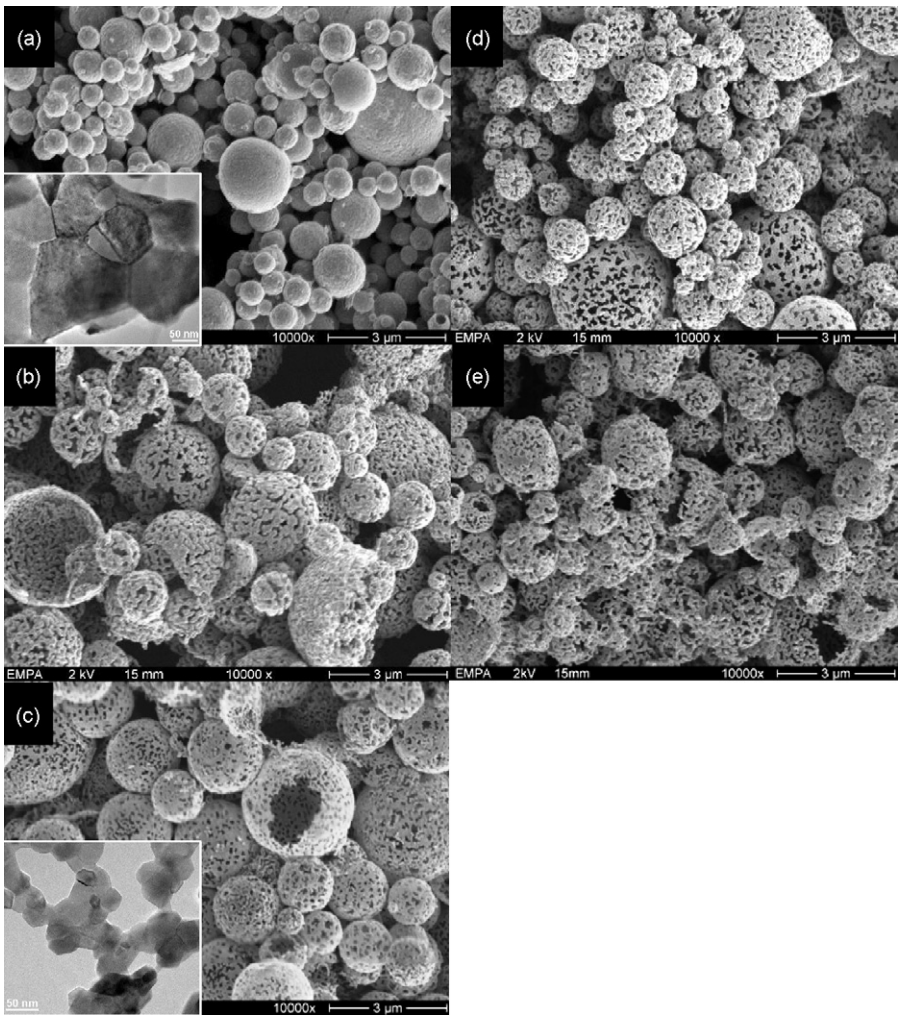

Fig. 1. SEM and TEM micrographs (inserts) of $LaMnO_3$ produced by USC from precursor solutions with 0.1 mol/l metal nitrates and increasing citric acid concentration: (a) no CA, (b) 0.1 mol/l, (c) 0.2 mol/l, (d) 0.4 mol/l, and (e) 0.8 mol/l. All samples were synthesized at 800 °C and calcined at 800 °C for 2 h. Samples a–e correspond to entries 1–5 in Table 1.

that we found in agreement with other works cannot be attributed uniquely to the use of water as solvent and nitrate precursors but specifically to the addition of CA, which is serving as the fuel.

Increasing CA concentration up to $M_{CA/MN} = 2$ was leading to a larger diameter of the spherical particles (on average) compared to the samples prepared without CA. Beside the particle size, there was an apparent change of the microstructure of the walls from Fig. 1b–e, that is the porosity of the particles walls changed especially for CA concentrations exceeding 0.2 mol/l. The effect of particle size growth and probably also the effect of change in the structure of the particle walls can be captured by analyzing the values of the BET specific surface area. Such data can also be used as qualitative assessment of optimal synthesis conditions since the surface area can significantly contribute to control the catalytic properties of perovskite-type oxides. The surface area of the calcined samples increased from 2.5 m^2/g (Fig. 1a) to 22 m^2/g (Fig. 1c) with the addition of CA, but when the $M_{CA/MN}$ exceeded 2, its value decreased to the level of $M_{CA/MN} = 1$ (ca. 11 m^2/g, Fig. 1d and e). The best $M_{CA/MN}$ ratio in this set of experiments appeared to be 2, resulting in a surface area of 22 m^2/g. The size of the hollow $LaMnO_3$ particles shown in Fig. 1c was in the range 0.6–3 μm.

Further SEM images are shown in Fig. 2 for the samples prepared from precursor solutions containing an overall metal concentration of 0.2 and 0.4 mol/l CA ($M_{CA/MN} = 2$) and with increasing oven temperature. The morphology of the as-prepared sample at 800 °C (Ts = 800 °C) is rather different from those prepared from the identical solution and calcined. The surface area of the as-prepared sample was about 40 m^2/g and dropped to ca. 16 m^2/g for the samples synthesized at 1100 °C. The surface area loss resulting from the increase of calcination temperature and the morphology change did not appear to be influenced by the different precursor solution concentration: the morphology shown in Fig. 2a was in fact characteristic of all the as-prepared samples produced with the addition of CA but not calcined. The spherical particles, on average similar in size to those of the calcined sample, appeared as polyhedra. Closer inspection of Fig. 2a revealed that some particles were rather amorphous indicating that the phase formation and crystallization process was yet not fully completed. Provided the relatively short residence time of the precursor solution droplets in the furnace at the given temperature, it is reasonable to conclude that the synthesis of $LaMnO_3$ by USC produced particles, which are partly amorphous or even contain some precursor residues. FT-IR spectra in the diffuse reflectance mode (DRIFT) and temperature programmed experiments (TPO) provided support to this observation from a chemical point of view.

Metal oxidic nanoparticles produced using spray methods often require a post-synthesis treatment in order to improve crystallinity of the final material and to accomplish complete decomposition of the precursors [24]. This last point emerges from the typical low residence time of droplets exposed to high temperatures. Fig. 3a displays the infrared spectra of the samples produced at 800 °C (Fig. 1c) and 1100 °C with a $M_{CA/MN}$ ratio of 2 and

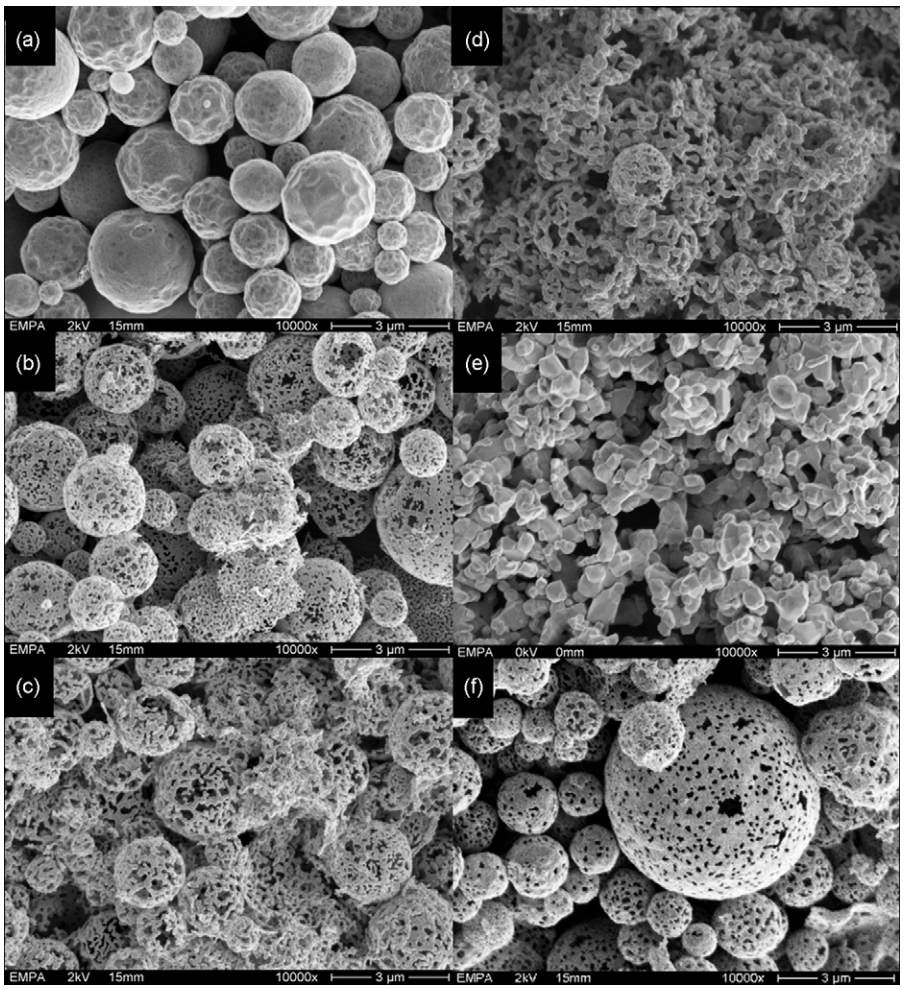

Fig. 2. SEM micrographs of $LaMnO_3$ powders generated from precursor solution containing 0.2 mol/l metal nitrates and 0.4 mol/l citric acid, (a) Ts = 800 °C, as-prepared; (b) Ts = Tc = 800 °C; (c) Ts = Tc = 900 °C; (d) Ts = Tc = 1000 °C; (e) Ts = Tc = 1100 °C; (f) Ts = 1100 °C, Tc = 800 °C. Calcination time was 2 h. Samples a–f correspond to entries 6–11 in Table 1.

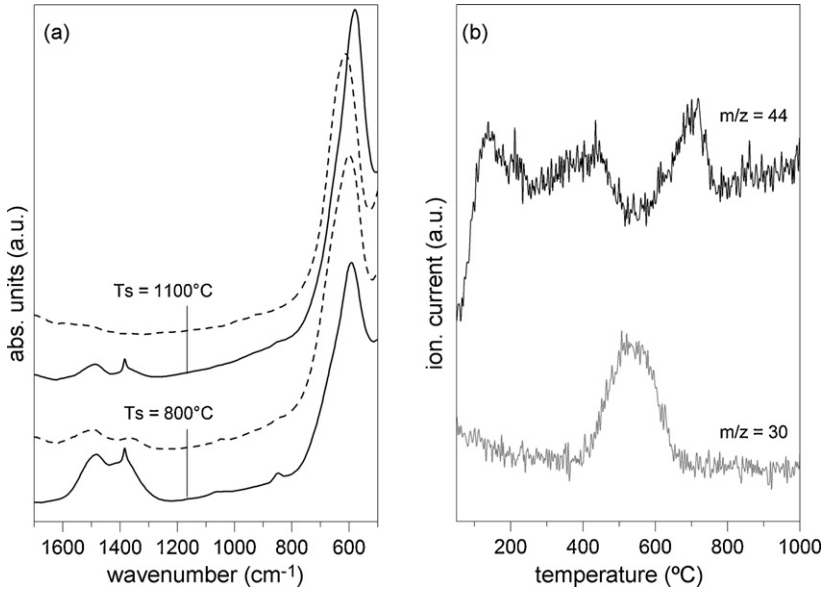

Fig. 3. (a) DRIFT spectra of as-prepared $LaMnO_3$ at 800 and 1100 °C (Ts, full line, entries 12 and 13 in Table 1) and calcined (Tc, dashed line, entries 5 and 16) at the temperature of synthesis for 2 h. Both samples were prepared from precursor solution containing C_{MN} = 0.1 mol/l and C_{CA} = 0.2 mol/l ($M_{CA/MN}$ = 2). (b) Profiles of MS signals during temperature programmed oxidation of $LaMnO_3$ (Ts = 800 °C; $M_{CA/MN}$ = 2, entry 12) from 50 to 1000 °C in 20 vol.% O_2/He.

C_{CA} = 0.2 mol/l, and of the same samples calcined at the temperature of synthesis. The features observed in Fig. 3 for both as-prepared and calcined samples were typical of all powders. All as-prepared samples exhibited various signals below 2000 cm^{-1}. The sharp signal at 1385 cm^{-1} is characteristic of ionic nitrates [45] and provided strong evidence for the presence of uncombusted nitrate species. The signals at 1483, 1370 and especially those at 1056 and 856 cm^{-1} identified carbonate species [46], which may have been produced during the high temperature synthesis as a result of combustion and/or have been adsorbed during cooling and exposure to air. Similar frequencies to those mentioned for carbonate-like species have been reported for various nitrate species adsorbed on perovskite-type oxides. Therefore, distinction between carbonates and nitrates in the 1500–1300 cm^{-1} spectral region appears not conclusive here. The absence of signals associated with uncombusted citrate species (additional strong signals above 1500 cm^{-1}) [11,47,48] indicated that these precursor species were fully combusted at the oven temperature of 800 °C. Higher furnace temperatures (Ts = 1100 °C in Fig. 3a) but otherwise identical synthesis conditions produced fewer residues. Calcination greatly improved the appearance of the spectra. Samples synthesized and calcined at the same temperature (Ts = Tc) exhibited improved surface purity in the spectral region 1700–1000 cm^{-1}. Only the samples with Ts = Tc = 800 °C still presented some residual signals at 1480 and 1370 cm^{-1} with lower intensity (carbonate species), which however were completely removed by calcination of samples with higher Ts and Tc than 800 °C. The sharp signal associated with ionic nitrate species observed on as-prepared powders completely disappeared. Calcination at intermediate temperature (500 °C, not shown) caused complete disappearance only of the ionic nitrates indicating that calcination at least at 800 °C should be considered for the as-prepared USC samples.

The signals observed below 1000 cm^{-1} are Mn–O vibrational modes of the MnO_6 octahedra of $LaMnO_3$ [49]. These signals also changed upon calcination at high temperature. The signal associated with the ν_3 stretch mode of the MnO_6 octahedra was spread over the 630–570 cm^{-1} frequency range, the low-energy limit being observed for the as-prepared samples and the high-energy limit for calcined powders. We assign this change to the improved crystallinity of the material by the aerobic calcination.

The profiles of MS traces corresponding to m/z = 30 and 44 recorded during oxidation from room temperature to 1000 °C of a representative $LaMnO_3$ sample (Ts = 800 °C; $M_{CA/MN}$ = 2) are shown in Fig. 3b. Desorption of CO_2 was characterized by a broad feature extending from 50 to 500 °C, which can be resolved in two desorption peaks at 133 and 430 °C, and a peak at 720 °C. This variety of desorption peaks may arise from decomposition of organic residues and most likely carbonate-like species displaying different adsorption strengths. A single broad peak centered at ca. 540 °C was observed in the case of the signal corresponding to NO (m/z = 30). Desorption of NO as from the TPO experiment confirms that the as-prepared samples received from the USC production contained nitrate species, in agreement with the infrared spectra reported in Fig. 3a. It should be noted that the features reported in Fig. 3b were common to all other samples in which desorption of CO_2 and NO was observed.

Fig. 3 demonstrates that the minimum calcination temperature required for the USC samples was 800 °C, a temperature at which the majority of the organic and inorganic residues of the precursors are efficiently removed from the powders.

After calcination at 800 °C (Fig. 2b) the polyhedral particles became porous (hollow), individual nano-sized perovskite particles became distinguishable and the morphology resembled that shown in Fig. 1b–e. Fig. 2b–e illustrates the influence of temperature on the particle morphology. The samples were produced from the same precursor solution (C_{CN} = 0.2 mol/l, C_{CA} = 0.4 mol/l) at the furnace temperature of 800, 900, 1000 and 1100 °C and were subsequently calcined at the same temperature of synthesis (Ts = Tc). The spherical structure of particles as in Figs. 1 and 2b gradually collapsed with the increase of temperature and the primary particles agglomerated into larger grains. No spherical structures could be observed for Ts = Tc = 1100 °C (Fig. 2e) and the average grain size was then ca. 500 nm.

It is remarkable that the X-ray diffractograms of all samples exhibited the reflections of the perovskite structure and all samples appeared single-phase; no reflections were found indicating the presence of secondary phases. The XRD data of selected $LaMnO_3$ samples prepared with C_{MN} = 0.1 mol/l and C_{CA} = 0.2 mol/l are given in Fig. 4. The bottom diffractogram of Fig. 4 shows that the as-prepared sample synthesized at the lowest temperature (800 °C) and not calcined was already crystalline and displayed orthorhombic geometry, suggesting an upper limit for the nonstoichiometry (δ) of 0.06 [50]. The relatively longer residence time (ca. 15 s) of the precursor droplets in the reactor tube compared to a previous report [40] allowed the formation of the perovskite-phase in a single step. However, the as-prepared samples still contained uncombusted residues and calcination not only removed the species observed in Fig. 3a but also modified the crystal structure of $LaMnO_3$. In agreement with the TEM images and with the changes associated with the M–O stretch signal in Fig. 3a, the crystallinity of the perovskite oxide changed after calcination and at increasing temperature (Ts, Tc). Formation of the rhombohedral $LaMnO_3$ structure clearly occurred at 900 °C, with some line splitting appearing already at 800 °C.

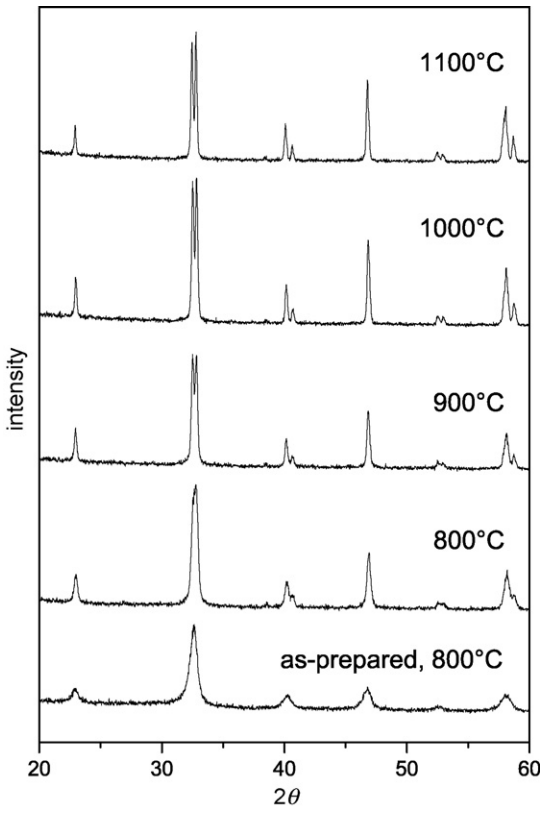

Fig. 4. X-ray diffraction patterns of the as-prepared $LaMnO_3$ (Ts = 800 °C, entry 12 in Table 1), and $LaMnO_3$ synthesized and calcined at 800, 900, 1000 and 1100 °C (entries 3, 14–16 in Table 1). All the samples were prepared from precursor solutions containing C_{MN} = 0.1 mol/l and C_{CA} = 0.2 mol/l.

3.2. Catalytic activity

The catalytic properties of the nano-structured powders were evaluated for methane combustion and activity was determined as a function of synthesis parameters, which were changed in order to optimize the structure of the USC powders. Therefore, the influence of addition of CA, of $M_{CA/MN}$ and of calcination at different temperatures was investigated. The activity is presented as the temperature at which methane conversion reached 50% (T_{50}). It should be noted that the hollow morphology of the USC powders observed by SEM (Figs. 1 and 2) was lost for the catalytic test, because of the processing of the materials into 150–200 μm particle agglomerates. This did not affect the nano-structure of the $LaMnO_3$ crystallites. Moreover, all samples were activated under oxygen at 500 °C prior to reaction and therefore samples, which were not treated after USC synthesis cannot be considered any longer as untreated. As demonstrated in Fig. 3, aerobic activation at 500 °C was not able to completely remove residues of the synthesis.

In order to inspect whether the calcination treatment (Tc) could be decisive for the catalytic property of USC powders, $LaMnO_3$ was synthesized at 1100 °C and calcined at 800 °C, for $M_{CA/MN}$ = 2 and precursor solution containing C_{MN} = 0.1–0.2 mol/l and C_{CA} = 0.2–0.4 mol/l. The structural and catalytic data are reported for simplicity in Table 1 for the case of a precursor solution with C_{MN} = 0.2 mol/l and C_{CA} = 0.4 mol/l. The morphology, surface area and catalytic activity for methane combustion were compared to that of the samples with no calcination (entry 17, Table 1) and with Ts = Tc = 1100 °C (entry 10) and Ts = Tc = 800 °C (entry 7). Fig. 2f clearly demonstrates that the morphology of the sample Ts = 1100 °C, Tc = 800 °C (entry 11) was similar to that of samples synthesized and calcined at lower temperature. Some degree of collapse of the $LaMnO_3$ skeleton of nanoparticles appeared. This morphology did not survive the treatment at 1100 °C (Ts = Tc, Fig. 2e; entry 10, Table 1). Calcination at the same high temperature of synthesis caused collapse of the structure and formation of large crystallites accompanied by an obvious drop of surface area to 2.3 m^2/g. However, the values of T_{50} are interesting and show that entry 11 has a comparable value to that of the sample not calcined, i.e. slightly above 500 °C. Entry 10 is considerably less active most probably due to its low surface area. The data reported in Table 1 indicate that the calcination temperature seems to be important to control the structural and catalytic properties of USC powders. This has to be attributed to the long calcination time (2 h) compared with the short residence time of the precursor micro-droplets in the USC equipment. The calcination is necessary to provide a stable material whose structure does not change in a non-controlled way during for example activation prior to reaction as it would be the case of the present powders not calcined. That Tc is important for catalytic activity should not diminish the importance of Ts. It should be emphasized that the powders with Ts = 1100 °C may still represent interesting materials in view of the need to apply high synthesis temperatures to obtain specific structures. Our data reveal that their activity can be tuned by changing Tc.

Fig. 5 displays the light-off curves of the $LaMnO_3$ samples produced without CA and with the addition of CA at increasing $M_{CA/MN}$. Therefore, the samples presented in Fig. 5 correspond to those presented in Fig. 1. $LaMnO_3$ generated from precursor solution at 800 °C without the addition of CA shows poor activity (T_{50} = 615 °C) and did not attain 100% conversion at 700 °C. Addition of CA resulted in the decrease of T_{50} by 70 °C at $M_{CA/MN}$ = 1, which is most likely related to the increase of surface area from 2.4 to 11.7 m^2/g and by 100 °C at $M_{CA/MN}$ = 2 (21.8 m^2/g) and 4 (11.6 m^2/g). Further increase of the concentration of chelating groups above $M_{CA/MN} > 2$ did not improve the catalytic properties

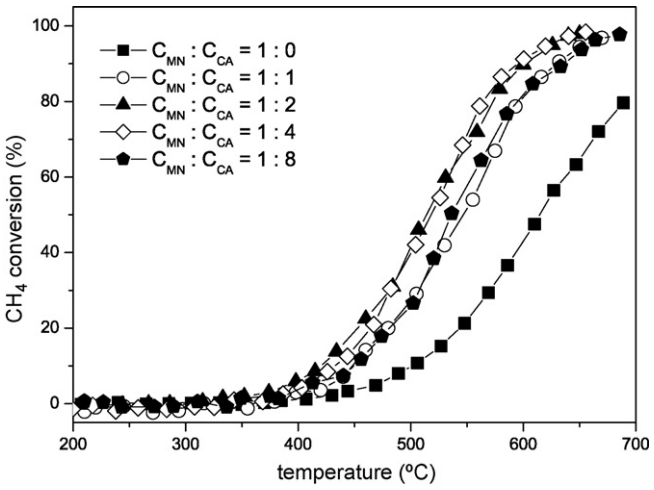

Fig. 5. Influence of CA concentration and $M_{CA/MN}$ ratio on the catalytic activity of $LaMnO_3$ samples prepared with Ts = Tc = 800 °C. Lines are drawn to guide the eye. Samples correspond to entries 1–5 in Table 1.

and even caused a decrease in activity, as in the case of $M_{CA/MN}$ = 8 (10.9 m^2/g). The surface area may play a central role but it is not the only factor. The addition of CA in sufficient excess can improve the morphology and catalytic activity of USC powders; however, the increase of the CA content also modifies the physical properties of the precursor solution, such as density, viscosity and surface tension, which might influence the formation of droplets and the final quality of the USC powders. Excess CA may cause the formation of dense particles due to higher local temperatures during the combustion process and hence change the aspect of the primary particles [40]. We observed that excess CA did not cause deposition of additional residues as infrared spectra (not shown) did not reveal a dramatic difference in the surface species when increasing CA concentration. However, at $M_{CA/MN} > 4$ the productivity seriously dropped.

The s-shaped conversion profiles of Fig. 5 are characteristic of a temperature dependent reaction mechanism. It is known that methane combustion on $LaMnO_3$ exhibits low temperature and high temperature regimes, which are depending on the availability and mobility of oxygen on the catalyst surface and in the lattice, respectively [51,52]. Though a mechanistic investigation of the influence of synthesis parameters on catalytic activity is out of the focus of this work, we speculate that the differences observed in the catalytic activity (T_{50}) are not only provided by the textural properties of the USC samples but also by the different availability of the two types of oxygen responsible for low and high temperature activity, which is determined in first approximation by the synthesis parameters.

Combining the observations from SEM, BET and catalytic activity, it was concluded that $M_{CA/MN}$ = 2 is the optimal ratio for the USC synthesis of $LaMnO_3$ perovskite-type oxides and this ratio was actually used to further produce the perovskite-type powders examined in this study. This finding may rationalize the use of the same $M_{CA/MN}$ ratio used for the fabrication of $CaMn_{1-x}Nb_xO_3$ thermoelectrics [36]. This ratio, with C_{CA} = 0.2 mol/l appears appropriate also from a practical point of view, since the quartz oscillators of the ultrasonic equipment are prone to damage under large acid concentration.

It should be noted that at $M_{CA/MN}$ = 2 a difference in catalytic activity was also observed for samples that were prepared by simultaneously increasing both the concentration of the metal ions and of the chelating agent. The $LaMnO_3$ powder generated from the precursor solution with a higher nitrate concentration (C_{MN} = 0.2 M vs. 0.1 M) displayed improved catalytic activity, T_{50}

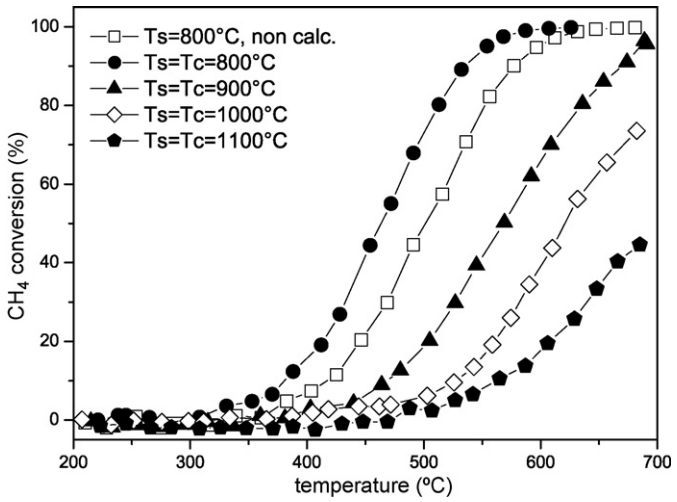

Fig. 6. Influence of calcination temperature on the catalytic activity of $LaMnO_3$ samples prepared under different conditions (entries 6–10 in Table 1): (□) Ts = 800 °C, as-prepared; (●) Ts = Tc = 800 °C; (▲) Ts = Tc = 900 °C; (◇) Ts = Tc = 1000 °C; (⬟) Ts = Tc = 1100 °C. $M_{CA/MN}$ = 2; C_{CA} = 0.4 mol/l, C_{MN} = 0.2 mol/l.

being further decreased by 50 °C (T_{50} = 470 °C). Therefore, the concentration of the metal ions in the precursor solution revealed an additional parameter to be optimized, but care should be taken not to excessively increase CA concentration, as mentioned above.

Further, the catalytic activity was tested for samples prepared with identical $M_{CA/MN}$ ratio (2) but increasing furnace temperature (800–1100 °C). The results are shown in Fig. 6. Activity towards methane combustion decreased significantly with increasing temperature, the difference in T_{50} between the low- and the high-temperature samples being of ca. 250 °C. This trend was independent of C_{CA} and C_{MN} and was most likely the result of the Ts–Tc combination and of the drop in surface area. The as-prepared sample (Ts = 800 °C, 38.3 m^2/g, orthorhombic) also displayed high activity but was still less active than the corresponding sample with Tc = 800 °C (16.8 m^2/g, rhombohedral), which displayed less than half of its surface area. In this case, the different crystal form of $LaMnO_3$ as displayed in Fig. 4 may be a decisive factor to determine the catalytic activity [53].

3.3. B-site and precious metals

Provided the optimal USC synthesis conditions determined for $LaMnO_3$ which was set as the reference material, the production of perovskite-type powders with different transition metal at B-site (Co and Fe) was undertaken from precursor solutions containing 0.1 mol/l metal nitrates and 0.2 mol/l CA at the oven temperature of 800 °C. The resulting nano-scale $LaFeO_3$ and $LaCoO_3$ powders were calcined in air at 800 °C. Similarly to $LaMnO_3$, $LaFeO_3$ and $LaCoO_3$ have attracted interest as potential catalysts for various catalytic applications, mainly related to environmental pollution control issues.

The X-ray diffractograms of $LaFeO_3$ and $LaCoO_3$ shown in Fig. 7 exhibited orthorhombic and rhombohedral structures, respectively. The values of the surface area of the Fe- (9.8 m^2/g, Table 2) and Co-containing (5.5 m^2/g) samples are clearly inferior to those found for $LaMnO_3$ samples. It is obvious that the optimal conditions used for preparing $LaMnO_3$ are not the same for the preparation of these two perovskite-type oxides. This is reflected in the SEM micrographs of the samples in Fig. 7, showing that the hollow structure is maintained in $LaFeO_3$ but with less porous particle walls, whereas it is lost in $LaCoO_3$.

The catalytic activity of $LaMnO_3$, $LaFeO_3$ and $LaCoO_3$ samples prepared by the USC method using identical conditions of precursors and CA concentration, Ts and Tc are reported in Fig. 8. The activity of a $LaMnO_3$ sample (16.7 m^2/g) prepared by the amorphous citrate method is also reported for comparison. The activity decreased in the order Mn > Co > Fe, in agreement with reported catalytic trends [54,55]. It is important to note that the two $LaMnO_3$ samples, fabricated by USC and by the amorphous citrate method, displayed comparable catalytic activity, which demonstrates the potential of the USC method as a simple synthesis route to catalytic materials. To this end, addition of precious metals as Pd and Pt to metal oxidic formulations is of interest for a wide range of catalytic applications. A central point with respect to the precious metal–perovskite combination lies in the control of coordination and state of the metal relative to the perovskitic support, since this may have tremendous effects on catalytic activity and may impart intriguing structural properties to the catalytic material [3].

As other spray synthesis methods, the USC provides a simple, clean, scalable and inexpensive route to the preparation of precious metal containing catalysts. Powders with a nominal formula $La(Mn,Pd)O_3$ and $La(Fe,Pd)O_3$ were prepared by partially substituting Mn or Fe with a Pd salt in the precursor solution so to obtain a defined precious metal loading. The analysis of the precious metal content by ICP-OES (Table 2) indicated that a small fraction of Pd was lost in $La(Mn,Pd)O_3$ as a consequence of the formation of a precipitate in the precursor solution. The particle morphology (Fig. 7) was retained in the Pd-containing samples. The state of palladium in these samples was determined by collecting X-ray absorption near-edge spectroscopy (XANES) data and by comparison with PdO. The white line of Pd in octahedral coordination (PdO_6 octahedra in $LaPdO_3$ [56]) is characteristic and substantially different from that of square planar Pd^{2+} in PdO and therefore can be used as a fingerprint for the assessment of the coordination of Pd within the samples. Fig. 9 shows the X-ray absorption spectra of $La(Mn,Pd)O_3$, $La(Fe,Pd)O_3$, PdO and Pd. The $La(Fe,Pd)O_3$ sample exhibited the typical double-peak feature of octahedrally coordinated Pd^{3+} indicating that Pd had been incorporated at the B-site within the ABO_3 structure. Convincing evidence for the incorporation of Pd in $LaFeO_3$ has been provided by Nishihata et al. [3]. $LaFeO_3$ has been shown to be an ideal host for Pd [57]. The ionic radius of Pd in the oxidation states $n \geq 2$ is stabilized by the perovskite and incorporation does not compromise the formation of the perovskite structure, according to the tolerance factor defined by Goldschmidt [58]. In the case of $La(Mn,Pd)O_3$, the white line is not unambiguously revealing Pd in a different environment and oxidation state than PdO as in the Fe-containing sample, but a closer inspection revealed that the spectrum did not really compare with that of PdO either. We tentatively conclude that Pd exhibited mixed coordination probably as the result of non-optimized synthesis conditions. The XRD data provided support for the presence of PdO in $La(Mn,Pd)O_3$ (not shown). A weak reflection at ca. $2\theta = 34°$ that was absent in $LaMnO_3$ prepared under identical conditions revealed the formation of PdO [59]. Moreover, this feature was not found in the diffractogram of $La(Fe,Pd)O_3$, which observation though not conclusive supported the complete incorporation of Pd in the perovskite framework of $LaFeO_3$. As it is the case for $La(Mn,Pd)O_3$, the production of Pd-containing samples could be further improved by controlling the conditions of preparation of the precursor solution, i.e. pH and polymerization time.

The conversion plots are shown in Fig. 8 and the data are summarized in Table 2 together with those of the Pd-free samples. Addition of Pd to $LaMnO_3$ and $LaFeO_3$ improved the catalytic activity towards methane combustion by lowering T_{50} by ca. 50 °C. The effect of Pd addition to perovskite-type oxides on catalytic

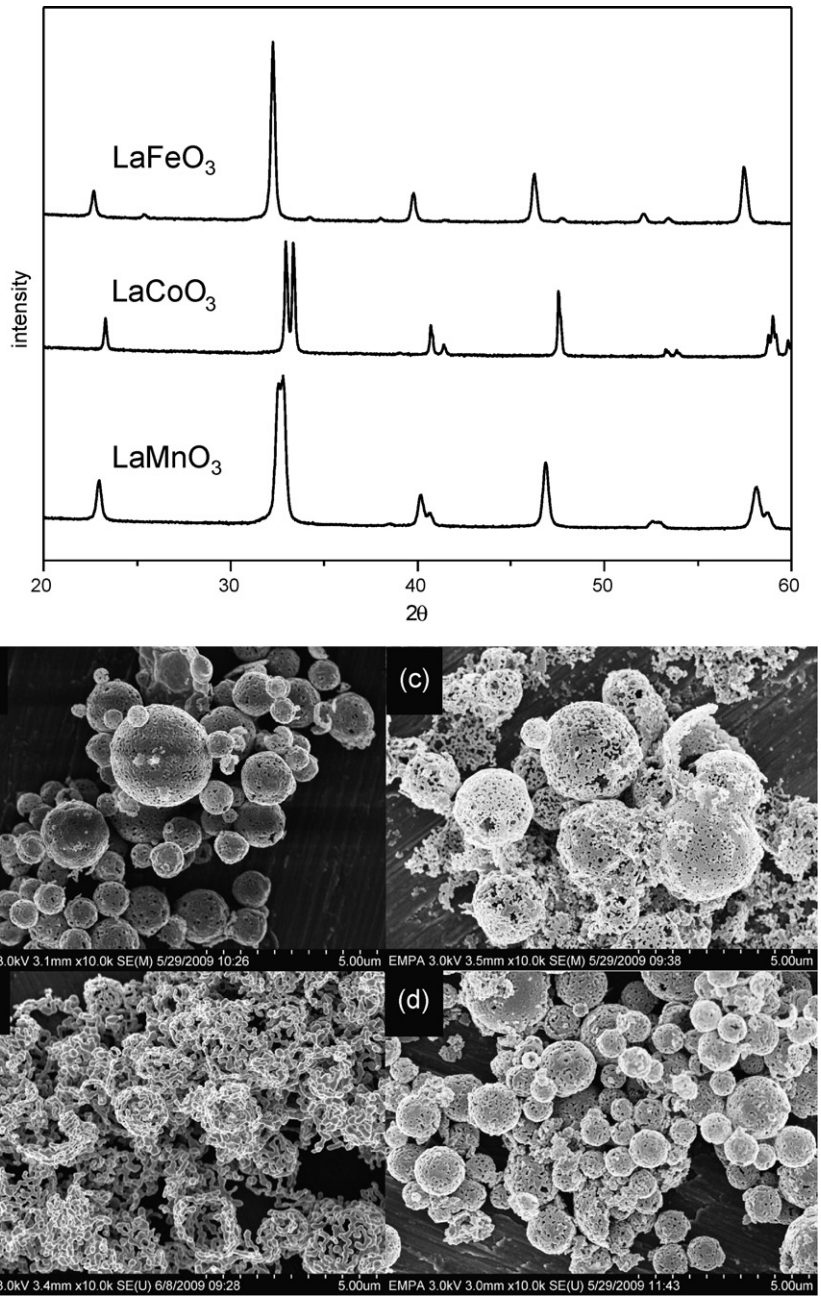

Fig. 7. Top panel: X-ray diffraction patterns of $LaMnO_3$, $LaCoO_3$ and $LaFeO_3$ synthesized and calcined at 800 °C. Bottom panel: SEM micrographs of (a) $LaFeO_3$, (b) $LaCoO_3$, (c) $La(Mn,Pd)O_3$ and (d) $La(Fe,Pd)O_3$. All the samples were prepared from precursor solutions containing C_{MN} = 0.1 mol/l and C_{CA} = 0.2 mol/l.

Table 2
Structural and catalytic properties of $LaBO_3$ (B = Mn, CO, Fe) and of $La(Mn,Pd)O_3$ and $La(Fe,Pd)O_3$ samples prepared from the same precursor solution (C_{MN} = 0.1 mol/l and C_{CA} = 0.2 mol/l).

Sample	Ts (°C)	Tc (°C)	Pd content		Surface area (m^2/g)	T_{50} (°C)[b]
			Nominal	Exp.[a]		
$LaMnO_3$	800	800			21.8	515
$LaMnO_3$[c]		800			16.7	525
$La(Mn,Pd)O_3$	800	800	2 wt.%	1.66 ± 0.07	13.4	482
$LaFeO_3$	800	800			9.8	625
$La(Fe,Pd)O_3$	800	800	1 wt.%	0.95 ± 0.04	9.6	570
$LaCoO_3$	800	800			5.5	560

[a] Determined by ICP-OES.
[b] Determined from catalytic measurements as indicated in Section 2.
[c] Prepared using the amorphous citrate method.

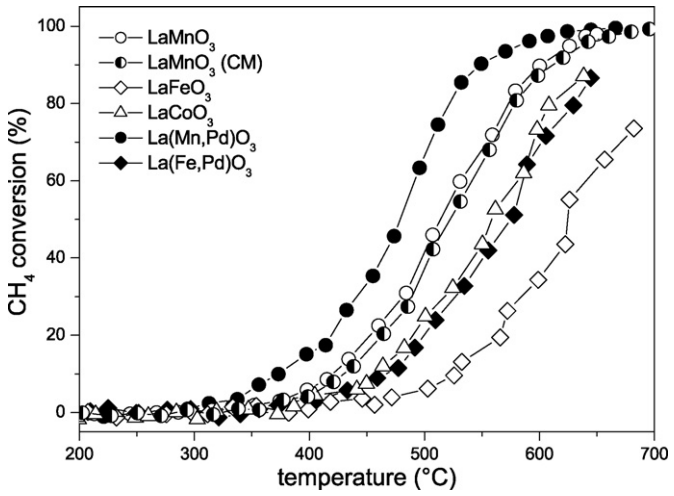

Fig. 8. Catalytic activity data for methane combustion of Mn-, Fe-, and Co-containing perovskite-type oxides prepared by USC, $LaMnO_3$ prepared by the amorphous citrate method and of Pd-containing samples prepared by USC. Lines are drawn to guide the eye.

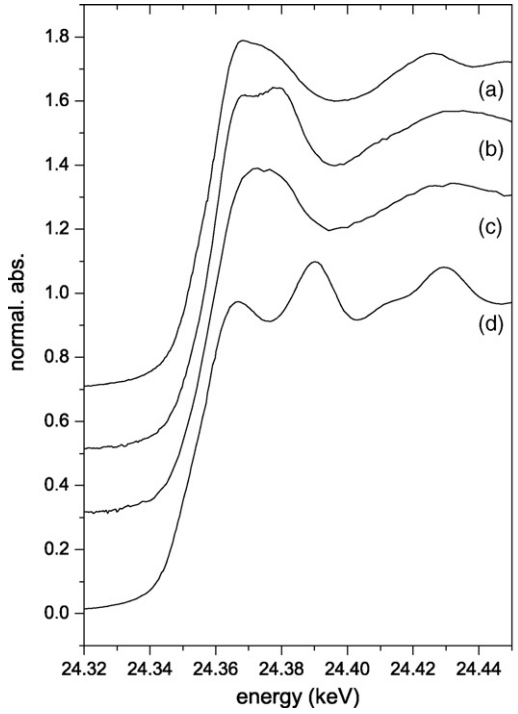

Fig. 9. XANES data recorded at the Pd K-edge for (a) PdO, (b) $La(Fe,Pd)O_3$, (c) $La(Mn,Pd)O_3$ and (d) Pd (foil).

activity towards methane combustion appears controversial. In Pd–$LaMnO_3$ no improvement was observed compared to $LaMnO_3$, unless the Pd–$LaMnO_3$ is subject to activation at high temperature [4] or reduced [60]. We have observed [61] no activity improvement for $La(Fe,Pd)O_3$, where Pd is fully incorporated within the perovskite framework, compared to $LaFeO_3$ in the case of samples prepared using a conventional amorphous citrate route. On the other hand, addition of Pd to $LaCoO_3$ [62], $LaMnO_3$ [63], $LaTi_{0.5}Mg_{0.5}O_3$ [64] and $La_{0.95}Ce_{0.05}CoO_3$ [65] was claimed to improve activity. The presence of Pd (nano-)particles supported on the perovskite-type oxide are most likely responsible for the activity improvement observed in several studies and are responsible for the improvement observed in the case of USC $La(Mn,Pd)O_3$. The case of $La(Fe,Pd)O_3$ prepared by USC in which octahedral Pd is occupying the B-site of $LaFeO_3$ deserves further attention but is outside the focus of this work.

4. Conclusion

USC is a reliable, simple and versatile method for the preparation of mixed oxides. The USC synthesis of $LaMnO_3$ perovskite was systematically investigated by varying the content of the precursor solution and adjusting the temperature of synthesis and calcination. The results show that the addition of citric acid in sufficient excess to the metal precursors leads to micro-sized powders with hollow spherical morphology and thin porous walls composed of nano-sized perovskite crystallites (30–50 nm).

As-prepared USC powders produced in the temperature range 800–1100 °C (Ts) were crystalline and exhibited large surface area (ca. 40 m^2/g) but yet not well-defined particle morphology. Improved crystallinity and well-defined particle morphology was obtained by applying a calcination step. Calcination is a necessary procedure to eliminate carbon-containing and nitrate residues, however still preserving the surface area at values interesting for catalytic applications (ca. 15–20 m^2/g). The calcination temperature Tc rather than the synthesis temperature Ts appeared to be critical to tune the catalytic activity of USC powders. For $LaMnO_3$, the optimal synthesis conditions based on textural properties, crystallinity and catalytic activity were fixed at Ts = Tc = 800 °C, with a CA-to-metal ions ratio of 2. Large excess of citric acid, as well as of metal ion precursors, can be unfavorable to USC, lowering the production rate and deteriorating the quality of USC powders. The catalytic activity for methane combustion for the sample prepared under these conditions was comparable to those of $LaMnO_3$ prepared by conventional methods. These conditions were also applied to produce $LaFeO_3$, $LaCoO_3$ and Pd-containing $LaMnO_3$ and $LaFeO_3$ by USC. The textural characterization and the activity tests demonstrated that additional optimization of the synthesis conditions may be required to improve the quality of the materials and their catalytic activity. Addition of Pd to $LaMnO_3$ and $LaFeO_3$ is an example of how the control of the synthesis conditions is critical to prepare materials with activity strongly depending of the state of the precious metal.

In conclusion, the potential of USC for the production of mixed oxide catalyst particles with defined crystallinity, morphology and textural properties has been demonstrated.

Acknowledgments

The authors gratefully acknowledge A. Eyssler for the preparation of $LaMnO_3$ by the amorphous citrate method, Dr. D. Logvinovich for the TEM measurements, P. Hinz for some SEM measurements and L. Rotach for providing support for the electronics of the USC equipment. X.W. would like to thank BNF at University of Bern for financial support. The Swiss-Norwegian beamline at ESRF is kindly acknowledged for providing beam time and support during measurement.

References

[1] M.A. Pena, J.L.G. Fierro, Chem. Rev. 101 (2001) 1981.
[2] A. Weidenkaff, Adv. Eng. Mater. 6 (2004) 709.
[3] Y. Nishihata, J. Mizuki, T. Akao, H. Tanaka, M. Uenishi, M. Kimura, T. Okamoto, N. Hamada, Nature 418 (2002) 164.
[4] S. Cimino, M.P. Casaletto, L. Lisi, G. Russo, Appl. Catal. A: Gen. 327 (2007) 238.
[5] E. Tzimpilis, N. Moschoudis, M. Stoukides, P. Bekiaroglou, Appl. Catal. B: Environ. 84 (2008) 607.
[6] W.F. Libby, Science 171 (1971) 449.
[7] R.J.H. Voorhoeve, D.W. Johnson, J.P. Remeika, P.K. Gallagher, Science 195 (1977) 827.

[8] N. Yamazoe, Y. Teraoka, Catal. Today 8 (1990) 175.
[9] E. Campagnoli, A. tavares, L. Fabbrini, I. Rossetti, Y.A. Dubitsky, A. Zaopo, L. Forni, Appl. Catal. B: Environ. 55 (2005) 133.
[10] M.S.G. Baythoun, F.R. Sale, J. Mater. Sci. 17 (1982) 2757.
[11] H. Taguchi, S. Matsu-ura, M. Nagao, J. Solid State Chem. 129 (1997) 60.
[12] J. Shu, S. Kaliaguine, Appl. Catal. B: Environ. 16 (1998) L303.
[13] Y. Teraoka, S. Nanri, I. Moriguchi, K. Shimanoe, N. Yamazoe, Chem. Lett. 29 (2000) 1202.
[14] A.E. Giannakas, T.C. Vaimakis, A.K. Ladavos, P.N. Trikalitis, P.J. Pomonis, J. Colloid Interf. Sci. 259 (2003) 244.
[15] F. Teng, W. Han, S. Liang, B. Gaugeu, R. Zong, Y. Zhu, J. Catal. 250 (2007) 1.
[16] G. Zou, L. Chen, X. Wang, Catal. Lett. 126 (2008) 96.
[17] A. Baiker, P.E. Marti, P. Keusch, E. Fritsch, A. Reller, J. Catal. 146 (1994) 268.
[18] J. Kirchnerova, M. Alifanti, B. Delmon, Appl. Catal. A: Gen. 231 (2002) 65.
[19] A. Civera, M. Pavese, G. Saracco, V. Specchia, Catal. Today 83 (2003) 199.
[20] G.L. Messing, S.C. Zhang, G.V. Jayanthi, J. Am. Ceram. Soc. 76 (1993) 2707.
[21] S.E. Pratsinis, Prog. Energy Combust. Sci. 24 (1998) 197.
[22] L. Fabbrini, I. Rossetti, L. Forni, Appl. Catal. B: Environ. 44 (2003) 107.
[23] G.L. Chiarello, I. Rossetti, L. Forni, J. Catal. 236 (2005) 251.
[24] G.L. Chiarello, J.D. Grunwaldt, D. Ferri, F. Krumeich, C. Oliva, L. Forni, A. Baiker, J. Catal. 252 (2007) 127.
[25] D. Peters, J. Mater. Chem. 6 (1996) 1605.
[26] J.H. Lee, K.Y. Jung, S.B. Park, J. Mater. Sci. 34 (1999) 4089.
[27] P. Fortunato, A. Reller, H.R. Oswald, Solid State Ionics 101 (1997) 85.
[28] Y.L. Song, S.C. Tsai, C.Y. Chen, T.K. Tseng, C.S. Tsai, J.W. Chen, Y.D. Yao, J. Am. Ceram. Soc. 87 (2004) 1864.
[29] W.H. Suh, K.S. Suslick, J. Am. Chem. Soc. 127 (2005) 12007.
[30] W. Kucza, J. Oblakowski, R. Gajerski, S. Labus, M. Danielewski, A. Malecki, J. Morgiel, A. Michalski, J. Therm. Anal. Calorim. 88 (2007) 65.
[31] P.S. Patil, Mater. Chem. Phys. 59 (1999) 185.
[32] C.H. Jung, D.K. Kim, J. Mater. Syn. Proc. 10 (2002) 23.
[33] J.P. Coutures, P. Odier, C. Proust, J. Mater. Sci. 27 (1992) 1849.
[34] K.K. Lee, Y.C. Kang, K.Y. Jung, J.H. Kim, J. Alloys Compd. 395 (2005) 280.
[35] W. Guo, A.K. Datye, T.L. Ward, J. Mater. Chem. 15 (2005) 470.
[36] L. Bocher, R. Robert, M.H. Aguirre, S. Malo, S. Hebert, A. Maignan, A. Weidenkaff, Solid State Sci. 10 (2008) 496.
[37] L. Bocher, M.H. Aguirre, R. Robert, M. Ttrottmann, D. Logvinovich, P. Hug, A. Weidenkaff, Thermochim. Acta 457 (2007) 11.
[38] C.R. Michel, E.R. Lopez, H.R. Zea, Mater. Res. Bull. 41 (2006) 209.
[39] A. Furusaki, H. Konno, R. Furuichi, J. Mater. Sci. 30 (1995) 2829.
[40] D.S. Jung, S.K. Hong, Y.C. Kang, J. Ceram. Soc. Jpn. 116 (2008) 141.
[41] M.T. Bore, T.L. Ward, A. Fukuoka, A.K. Datye, Catal. Lett. 98 (2004) 167.
[42] B. Savreux, L. Bocher, M. Trottmann, A. Weidenkaff, unpublished data.
[43] S. Specchia, A. Civera, G. Saracco, V. Specchia, Catal. Today 117 (2006) 427.
[44] T.J. Ressler, Syn. Rad. 5 (1998) 118.
[45] C.C. Addison, B.M. Gatehouse, J. Chem. Soc. (1960) 613.
[46] G. Busca, V. Lorenzelli, Mater. Chem. 7 (1982) 89.
[47] H.M. Zhang, Y. Teraoka, N. Yamazoe, Chem. Lett. (1987) 665.
[48] Y. Li, L. Xe, L. Fan, Y. Yan, J. Alloys Compd. 478 (2009) 493.
[49] K. Li, X. Li, K. Zhu, J. Zhu, Y. Zhang, J. Appl. Phys. 81 (1997) 6943.
[50] J. Töpfer, J.B. Goodenough, J. Solid State Chem. 130 (1997) 117.
[51] T. Seiyama, Catal. Rev. Sci. Eng. 34 (1992) 281.
[52] R. Hammami, S.B. Aissa, H. Batis, Appl. Catal. A: Gen. 353 (2009) 145.
[53] G. Saracco, F. Geobaldo, G. Baldi, Appl. Catal. B: Environ. 20 (1999) 277.
[54] H. Arai, T. Yamada, K. Eguchi, T. Seiyama, Appl. Catal. 26 (1986) 265.
[55] I. Rossetti, O. Buchneva, C. Biffi, R. Rizza, Appl. Catal. B: Environ. 89 (2009) 383.
[56] S.-J. Kim, S. Lemaux, G. Demazau, J.-Y. Kim, J.-H. Choy, J. Mater. Chem. 12 (2002) 995.
[57] H. Tanaka, M. Taniguchi, M. Uenishi, N. Kajita, I. Tan, Y. Nishihata, J. Mizuki, K. Narita, M. Kimura, K. Kaneko, Angew. Chem. Int. Ed. 45 (2006) 5998.
[58] V.M. Goldschmidt, Skr. Nor. Videnk.-Akad., Kl. 1: Mat. Naturvidensk. Kl. 8, 1926.
[59] H. Zhang, J. Gromek, G.W. Fernando, S. Boorse, H.L. Marcus, J. Phase Equilibria 23 (2002) 246.
[60] L. Giebeler, D. Kiessling, G. Wendt, Chem. Eng. Technol. 30 (2007) 889.
[61] A. Eyssler, P. Hug, D. Ferri, R. Figi, A. Weindekaff, in preparation.
[62] B. Kucharczyk, W. Tylus, Catal. Today 90 (2004) 121.
[63] B. Kucharczyk, W. Tylus, Catal. Today 137 (2008) 318.
[64] S. Petrovic, L. Karanovic, P.K. Stefanov, M. Zdujic, A. Terlecki-Baricevic, Appl. Catal. B: Environ. 58 (2005) 133.
[65] Y. Wu, L. Luo, React. Kinet. Catal. Lett. 93 (2008) 305.